Dynamical properties of the repressilator model

Olguta Buse and Rodrigo Pérez
Department of Mathematical Sciences, IUPUI, 402 N. Blackford Street, Indianapolis, Indiana 46202, USA

Alexey Kuznetsov
Department of Mathematical Sciences and Center for Mathematical Biosciences, IUPUI, 402 N. Blackford Street, Indianapolis, Indiana 46202, USA

(Received 26 June 2009; revised manuscript received 19 November 2009; published 11 June 2010)

Oscillatory regulatory networks have been discovered in many regulatory pathways. Due to their enormous complexity, it is necessary to study their dynamics by means of highly simplified models. These models have received particular value because artificial regulatory networks can be engineered experimentally. In this paper, we study dynamical properties of an artificial regulatory oscillator called repressilator. We have shown that oscillations arise from the existence of an absorbing toruslike region in the phase space of the model. This geometric structure requires monotonic repression at all promoters and the absence of any regulatory connections apart from a cyclic repression loop. We show that oscillations collapse as only weak extra connections are introduced if there is imbalance between the attended concentrations and those sufficient for saturation of the promoters. We found that a pair of diffusively coupled repressilators displays synchronization properties similar to those of relaxation oscillators if the regulatory connections in the cyclic repression loop are strong. Thus, the role of strengthening these connections can be viewed as introducing time scale separation among variables. This may explain controversial synchronization properties reported for repressilators in earlier studies.

DOI: 10.1103/PhysRevE.81.066206 PACS number(s): 05.45.Xt, 87.18.Cf

I. INTRODUCTION

Regulatory molecular networks are collections of interacting molecules in a cell. One particular kind, oscillatory networks, has been discovered in many pathways. Well-known examples are the circadian clock [1] and the cell cycle [2], where the oscillatory nature of the process plays a central role. Regulatory oscillators are also found in many other networks including apoptotic [3], metabolic [4], and morphogenic [5,6] pathways. Abnormalities of these processes lead to various diseases, from sleep disorders to cancer. For this reason, the regulatory oscillators attract significant attention among biologists and biophysicists.

Since these natural regulatory networks are very complex, it is necessary to study their dynamics by means of highly simplified models. These models are particularly valuable because *artificial* regulatory networks can be engineered experimentally. Switches [7,8], oscillators [7,9], and noise-dampening networks [10] have been synthesized to prove that a regulatory network can be decomposed into simple functional elements to control complex biochemical systems (see, e.g., [11–13]). The qualitative agreement between models and experiments is remarkable and validates the mathematical approach to the analysis of regulatory networks.

Modeling studies suggest several designs for artificial oscillatory networks. There are many implementations of hysteresis-based oscillators [7,15–17]. Another artificial oscillatory network called the repressilator [9] borrows from engineering the idea of a ring oscillator. The mechanism is based on connecting an odd number of inverters (negative control elements) in a ring. Its genetic implementation uses three proteins that cyclically repress the synthesis of one another. Our computational study [18] suggests that the oscillatory mechanism of the repressilator is qualitatively different from that in other genetic oscillators. In particular, the distinctions between the oscillatory mechanisms are that one requires bistability in a subnetwork and separation of time scales, whereas the other does not use bistability and requires all time scales to be similar. Recently, we have proven existence of a limit cycle in the repressilator model [19]. The proof reveals structural properties of the model that are responsible for the appearance of periodic behavior. In this paper, we analyze the requirements for realization of the repressilator oscillatory mechanism and discuss how the distinct dynamical properties of the repressilator are related to its structure.

II. MODEL

The idea for the oscillatory mechanism of the repressilator is the cyclic repression of protein synthesis as shown in Fig. 1. The following system of equations describes the behavior of the repressilator:

$$\frac{dm_1}{dt} = -m_1 + \frac{\alpha}{1+v^n} + \alpha_0,$$

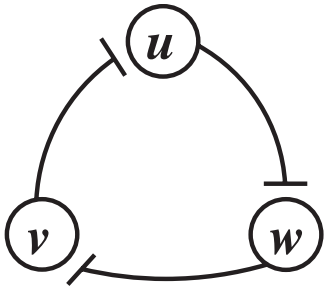

FIG. 1. The original Repressilator mechanism.

$$\frac{dm_2}{dt} = -m_2 + \frac{\alpha}{1+w^n} + \alpha_0,$$

$$\frac{dm_3}{dt} = -m_3 + \frac{\alpha}{1+u^n} + \alpha_0,$$

$$\frac{du}{dt} = -\beta(u - m_1),$$

$$\frac{dv}{dt} = -\beta(v - m_2),$$

$$\frac{dw}{dt} = -\beta(w - m_3). \quad (1)$$

Here, u, v, and w are proportional to protein concentrations, while m_i are proportional to the concentrations of mRNA corresponding to those proteins. All negative terms in the right-hand side represent degradation of the molecules. The nonlinear function $f(x)=\frac{\alpha}{1+x^n}$ reflects synthesis of the mRNAs from the DNA controlled by regulatory elements called promoters. n is called cooperativity and reflects multimerization of the protein required to affect the promoter. The three proteins are assumed to be identical, making the model symmetric. The mRNA concentrations are normalized by their translation efficiencies to remove extra parameters at m_i in the equations for the proteins. Additionally, the time is scaled in units of the mRNA lifetime, removing extra coefficients at m_i in the equations for the mRNA concentrations.

The system and the diagram present a highly simplified model of the oscillatory network. In particular, intermediate reaction steps such as binding of an effector to a promoter are assumed to be very fast and, therefore, are not explicitly shown in the model. The parameter α_0 represents uncontrolled (leaky) gene expression from the promoters. The ratio β between the decay rates of proteins and mRNAs is a small parameter which makes the dynamics of protein concentration much slower than that of mRNA. The system has been shown to oscillate both in experiments and in simulations for $n>2$ and big enough α.

To investigate the oscillatory mechanism in the system, we first reduce its dimension: Given that $\beta \ll 1$, the explicit inclusion of the mRNA concentration variables into the model is not essential. In fact, there is no significant difference in dynamics if the mRNA concentrations are assumed to be at their quasiequilibria, expressed by the algebraic relations

$$m_1 = \frac{\alpha}{1+v^n} + \alpha_0, \quad m_2 = \frac{\alpha}{1+w^n} + \alpha_0, \quad m_3 = \frac{\alpha}{1+u^n} + \alpha_0.$$

By this algebraic substitution, we arrive at a three-dimensional system that captures the oscillatory dynamics. Next, the uncontrolled part of the mRNA synthesis is usually small and, therefore, can be omitted ($\alpha_0=0$). As a result, we obtain the following dynamical system for further consideration

$$\frac{du}{dt} = \frac{\alpha}{1+v^n} - u,$$

$$\frac{dv}{dt} = \frac{\alpha}{1+w^n} - v,$$

$$\frac{dw}{dt} = \frac{\alpha}{1+u^n} - w. \quad (2)$$

Note that several assumption made for the initial model are not necessary for the reduced system. In particular, there is no need to assume that the dynamics of all mRNAs is the same, and, consequently, β may be assumed different, but small. We return to the discussion of symmetry in the concluding sections.

III. RESULTS

A. Geometric structure of the phase space

In this section, we describe the structure of the phase space that gives rise to oscillations in the repressilator model. The description is based on rigorous analysis of the system published in [19].

All trajectories are absorbed into a trapping cube. First, we show that there is a finite region in the phase space that attracts all trajectories. System [Eq. (2)] has an obvious symmetry by cyclic permutation of the three variables. This allows us to consider only one of the three, and the absorption is established analogously for the other two variables. When $u=0$, the u variable is increasing because $\frac{du}{dt}=\frac{\alpha}{1+v^n}>0$. When $u=\alpha$, u is decreasing because $\frac{du}{dt}=\alpha(\frac{1}{1+v^n}-1)<0$. Moreover, it is easy to see that for $u>\alpha$ the derivative does not become smaller in absolute value than certain quantity ε ($\frac{du}{dt}\leq -\varepsilon<0$ for all $u>\alpha$). As a result, the u variable is eventually trapped in the interval $(0,\alpha)$. The same statement holds for the v and w variables. Therefore, all trajectories of the system are absorbed into a *trapping cube* consisting of all (u,v,w) with $0<u,v,w<\alpha$.

The symmetry greatly simplifies the picture, but obviously is not necessary for the existence of the trapping region. In particular, if we introduce different parameters $\alpha_1,\alpha_2,\alpha_3$ in system [Eq. (2)], then the trapping region is a parallelogram with sides α_1, α_2, and α_3, respectively. The major reason for the existence of the trapping region is the dominance of degradation over synthesis for high concentrations of the components. The nonlinear functions in system [Eq. (2)], which represent synthesis of components, stay below α. By contrast, the negative terms, which represent degradation, can grow without saturation. Therefore, the existence of a trapping region is a consequence of limited synthesis and of the nonsaturable degradation of components.

The only equilibrium state is unstable for big enough α. Next, we investigate dynamics of the system within the trapping region. In the simplest case a stable equilibrium state exists, and a stationary concentration of all components sets in. The equilibrium is located at the intersection of the null

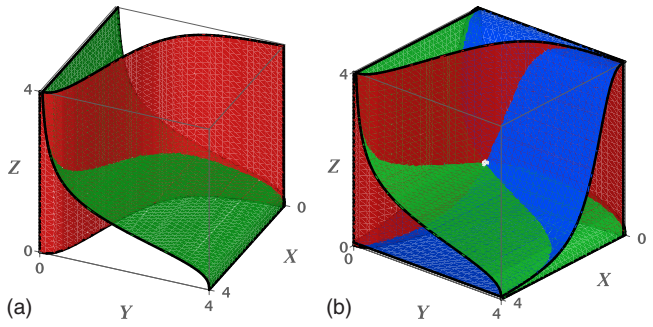

FIG. 2. (Color online) (A) The null surfaces N_u and N_v intersect along a monotonic curve. (B) The intersection of the three null surfaces is a single point R ($\alpha=4$, $n=3$).

surfaces N_u, N_v, N_w for all three equations. Separately, each null surface is the locus of points where one of the derivatives $\frac{du}{dt}, \frac{dv}{dt}, \frac{dw}{dt}$ is zero; see Fig. 2.

$$\frac{du}{dt} = 0 \Rightarrow N_u = \left\{ \frac{\alpha}{1+v^n} = u \right\},$$

$$\frac{dv}{dt} = 0 \Rightarrow N_v = \left\{ \frac{\alpha}{1+w^n} = v \right\},$$

$$\frac{dw}{dt} = 0 \Rightarrow N_w = \left\{ \frac{\alpha}{1+u^n} = w \right\}.$$

The intersection of two null surfaces is a monotonic curve. To find equilibrium states, we look for intersections of this curve with the remaining null surface. This results in the following equation:

$$f\{f[f(x)]\} - x = 0, \tag{3}$$

where, $f(x)=\frac{\alpha}{1+x^n}$. A solution of Eq. (3) exists because the left-hand side is positive when $x=0$ and negative when $x \to \infty$. Since $f'(x)=\frac{-\alpha n x^{n-1}}{(1+x^n)^2} < 0$, the derivative of the left-hand side of Eq. (3) is everywhere negative, and the left-hand side is monotonically decreasing. As a result, the solution to Eq. (3) is unique. Therefore, there is a single equilibrium state in the system for any parameters $\alpha > 0$ and $n > 1$.

To conduct bifurcation analysis of the equilibrium state, we notice first that the symmetry of the system forces the equilibrium to belong to the diagonal $\{u=v=w\}$. Then, the location of the equilibrium state is (r,r,r), where r satisfies

$$\frac{\alpha}{1+r^n} = r, \tag{4}$$

i.e., $r^{n+1}+r-\alpha=0$. The linearized system at the equilibrium state has eigenvalues (see [19])

$$\lambda_1 = -\frac{nr^n}{1+r^n} - 1,$$

$$\lambda_{2,3} = \left[\cos\left(\frac{\pi}{3}\right) \pm i \sin\left(\pm\frac{\pi}{3}\right) \right] \frac{nr^n}{1+r^n} - 1$$

$$= \left(\frac{n}{2}\frac{r^n}{1+r^n} - 1 \right) \pm i \left(\frac{\sqrt{3}n}{2}\frac{r^n}{1+r^n} \right). \tag{5}$$

The first eigenvalue is negative for any value of the parameters and corresponds to a stable eigendirection along the diagonal. In fact, the diagonal is the stable manifold of the equilibrium state not only locally as shown by the linearization, but also globally in the original system [Eq. (2)].

The plane of the complex eigenvectors is orthogonal to the diagonal due to symmetry. The real part of $\lambda_{2,3}$ changes monotonically between -1 and $\frac{n}{2}-1$ as the position of the equilibrium state r shifts from 0 to ∞ due to variations in α. In particular, Re $\lambda_{2,3}$ is always negative for $n \leq 2$. This agrees well with computer estimates performed in the original repressilator system [9]. A threshold value for n required for oscillations was also found in models of circadian clock [20].

For $n > 2$, there is a value $r_0=\sqrt{\frac{2}{n-2}}$ such that Re $\lambda_{2,3}$ is negative for $r < r_0$ and positive for $r > r_0$. The position of the equilibrium state depends on α. Below $\alpha_{\text{bif}}=r_0^{n+1}+r_0$, the equilibrium state is stable. Above this value, it becomes unstable via an Andronov-Hopf bifurcation. Our computation of the first Lyapunov coefficient at the equilibrium state shows that this coefficient is negative for any $n > 2$. Therefore the bifurcation is always supercritical, and it results in a stable (attracting) limit cycle for $\alpha > \alpha_{\text{bif}}$.

Trajectories are channeled into a toruslike region inside the trapping cube. Periodic behavior that corresponds to the limit cycle could in principle lose stability with further increase in α, giving rise to more complex oscillatory solutions. On the other hand, the repressilator model displays only periodic dynamics in simulations. Therefore, we further analyze the structure of the phase space that underlies oscillations.

The three null surfaces N_u, N_v, N_w divide the trapping cube into eight regions [Fig. 2(B)]. The structure is qualitatively equivalent to the splitting of three-dimensional space into octants by coordinate planes. Using this analogy, we call the eight parts of the cube *octant regions*. Since they are separated by the null clines, any point inside each octant region has the same pattern of signs for the derivatives $\frac{du}{dt}$, $\frac{dv}{dt}$, $\frac{dw}{dt}$. Therefore, any octant region can be described by a triple of signs "+" or "−." To represent a point exactly on a null surface, we include "∘" in the list of the symbols. For instance, (+++) represents the octant region near the origin where $\frac{du}{dt}, \frac{dv}{dt}, \frac{dw}{dt} > 0$. It is bounded by portions of the N_u, N_v, and N_w null surfaces represented by (∘++), (+∘+), and (++∘), respectively. The equilibrium state can be represented as (∘∘∘).

We mentioned already that the stable manifold of the equilibrium state coincides with the main diagonal [which crosses the cube from (−−−) to (+++)]. Nearby trajectories come close to the equilibrium state, and then are repelled along the plane orthogonal to the diagonal because the equilibrium is a saddle point (Fig. 3). More generally, we prove that

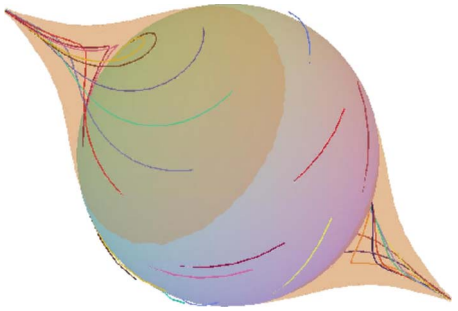

FIG. 3. (Color online) The construction of the spindle. The spindle consists of trajectory segments through all points of the sphere surrounding the equilibrium state.

(a) Every orbit in (−−−) or (+++) other than the diagonal escapes into the octant regions (+−−), (++−), (−+−), (−++), (−−+), (+−+), and remains trapped in these *lateral* regions. For example, along the portion (∘++) of the N_u-null surface, the vector field is directed from (+++) to (−++).

To rule out the possibility of orbits that return close to the equilibrium state, we construct a neighborhood S of the equilibrium state such that:

(b) A trajectory can only enter S from deep inside the octants (+++) and (−−−).

(c) Any trajectory (except for the diagonal) exits S only into the lateral regions.

The naive choice of a ball around the equilibrium state does not work because the trajectories can exit and enter the ball before deciding to stay in the lateral regions. This failed attempt indicates the correct construction for S. We take the ball and add those segments of trajectories that exit and reenter the ball (see Fig. 3). We call the resulting object S a *spindle* (see [18] for more details). Removing S from the union of the lateral pieces leaves a toruslike region T (see Fig. 4). Together, (a)–(c) show that every trajectory (except the diagonal) is eventually trapped in T, and the equilibrium state is far from T.

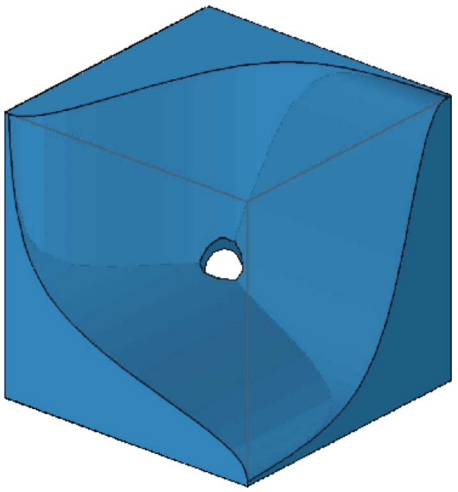

FIG. 4. (Color online) The six lateral octants meet at the equilibrium point R. Removing the spindle (which surrounds R) leaves the displayed region, which absorbs trajectories and has the topology of a torus.

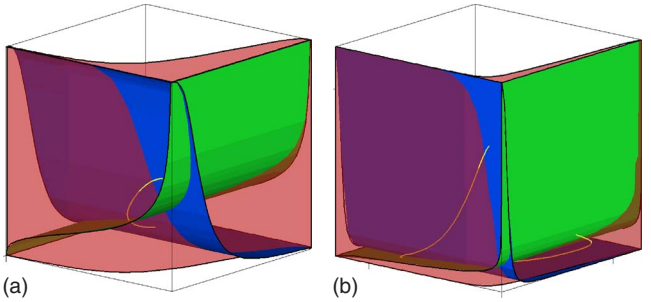

FIG. 5. (Color online) Trajectories and null clines in the cases of low and high α. (A) $\alpha=5$; (B) $\alpha=35$. Note that the torus stretches along the walls of the trapping cube.

Trajectories constantly move in a cyclic manner inside the absorbing torus. Next we determine how a trajectory moves inside the torus. The torus is composed of six pieces corresponding to the octant regions truncated at the equilibrium state. We adopt the same notation for torus pieces as for the octant regions. A trajectory cannot stay within any one torus piece. This follows from the monotonic changes in variables and the fact that the speed of change does not become arbitrarily small inside any torus piece. Each piece is bounded by five surfaces; two of them are boundaries of the trapping cube and the spindle, respectively. The torus piece can only absorb trajectories through these two boundaries. The other three surfaces are parts of the null clines N_u, N_v, and N_w. In particular, for the torus piece (+−+), these are (∘−+), (+∘+), and (+−∘). The boundary (+∘+) separates the torus piece with (+++) octant region, and, consequently, the trajectory may cross only into the torus. The remaining two boundaries separate pieces within the torus. Calculating the direction of the vector field on the boundaries, we have shown that the trajectory enters the piece through (∘−+) and escapes through (+−∘). As a result, the (+−+) piece absorbs trajectories from (−−+) and repels them into (+−−) within the torus. Repeating this analysis for other torus pieces, we determine that the only sequence in which a trajectory may flow is

$$(+-+)\mapsto(+--)\mapsto(+++)\mapsto(-+-)\mapsto(-++)\mapsto(---)\mapsto(+-+). \tag{6}$$

Therefore, *once trapped in the torus, the trajectory moves among torus pieces in a cyclic sequence.*

The cyclic motion of the trajectory result in the existence of a Poincaré return map from any boundary between torus pieces to itself. By Brower's Fixed Point Theorem, the system has a limit cycle. However, the stability or uniqueness of the limit cycle remains to be proven.

B. Synchronization properties of the repressilator depend on α

We noted that the shape of the limit cycle changes qualitatively as α increases (see Fig. 5). At high α, dynamics resembles relaxation oscillations, in which the shape of the limit cycle becomes not rounded, and there are fast and slow phases in the trajectory. Relaxation oscillations have been

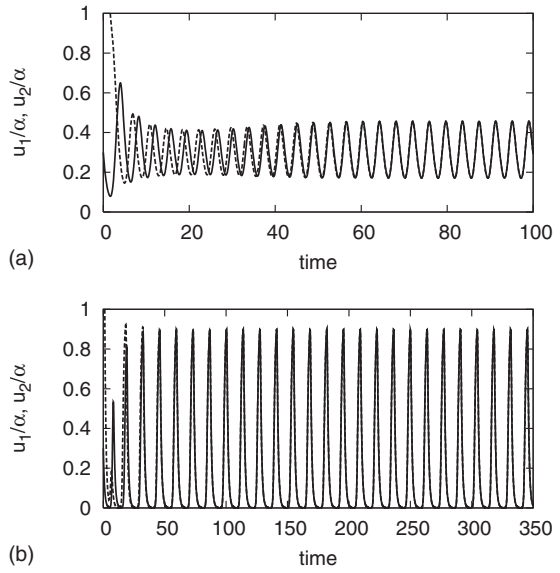

FIG. 6. Transient to synchronization in a pair of diffusively coupled repressilators. (a) At $\alpha=5$, the oscillators synchronize within multiple cycles. (b) At $\alpha=500$, the oscillators synchronize within only a couple of cycles. $d=0.1$. The time interval is chosen to match the number of oscillatory cycles in these two cases.

shown to synchronize faster than smooth oscillations [24]. To test this property, we couple two identical repressilators.

Each repressilator represents concentration changes in an isolated cell. In the literature, there are different ways to couple the cells in a population. All of them use an intercell signaling via quorum sensing mechanism [21]: that is, they use the diffusion of a small molecule, the autoinducer. However, some works [14,22] suggest addition of a subnetwork that provides coupling to each of the cells, whereas other works include the quorum sensing system into the regulatory network for the oscillator [15,18]. We adopt the latter approach because it introduces much less complexity into the system, e.g., there are fewer parameters to be examined. In the assumption of a dense population, the transmission of the coupling signals (diffusion) occurs in a fast time scale. No additional coupling variable is needed, and we arrive at the equations

$$\frac{du_i}{dt} = \frac{\alpha}{1+v_i^n} - u_i + d(u_j - u_i),$$

$$\frac{dv_i}{dt} = \frac{\alpha}{1+w_i^n} - v_i,$$

$$\frac{dw_i}{dt} = \frac{\alpha}{1+u_i^n} - w_i, \tag{7}$$

where i is the index of the cell. For the basic population of two cells, $i=1,2$, $j=2,1$. This is a six-dimensional system, in which the equations for each oscillator are the same [Eq. (2)], except for the additional coupling terms in the u_i equations. The parameter d is the strength of the coupling and represents diffusion between the cells. Figure 6 compares transients to synchrony for the pair with moderate and high α at the same coupling strength d. In the case of high α, the repressilators synchronize within a couple of cycles, whereas it takes many cycles in the case of moderate α. At high α, the synchronization properties of the repressilator match those observed for relaxation oscillators. Thus, the synchronization properties of the repressilator change according to the value of the parameter α.

IV. DISCUSSION

From computer simulations we know that the behavior remains periodic for arbitrarily high α. Our analysis excludes the possibility of chaotic dynamics emerging form a homoclinic connection of the saddle equilibrium state. This is because the stable manifold of the saddle is the diagonal, and that no nearby trajectory returns to a vicinity of the diagonal. Quasiperiodic behavior (*invariant* torus [23]) can also be excluded since the divergence of the vector field is negative everywhere. However, a cascade of period doubling bifurcations of limit cycles is still not excluded by the analysis. A proof of uniqueness and stability of the limit cycle will clarify what structural properties of the system determine the regularity of the dynamics.

Our proof of existence of the limit cycle gives a qualitative explanation of the oscillatory mechanism of the repressilator: the oscillations arise from circulation of the trajectories inside the absorbing torus. The symmetry of the system is not essential for the existence of the torus because it is only based on the monotonicity of the null surfaces, which reflects monotonic repression at the promoters. The fact that each equation depends only on two out of three variables was used to prove that the torus is a trapping region. So, if an activating term like $\frac{\alpha_1 w^n}{1+w^n}$ is introduced in the u equation of system [Eq. (2)], then trajectories from $(+--)$ may escape into $(---)$. If a repression term is introduced, the torus remains an absorbing region, but the cyclic motion along a sequence of torus pieces may not hold. For instance, if the term $\frac{\alpha_2}{1+w^n}$ is introduced into the u equation, a trajectory may return from $(+-+)$ to $(--+)$. The change also introduces new equilibria, the absence of which was used to prove continuous cycling inside the torus. This shows that the oscillatory mechanism is based on monotonic repression at the promoters and on the absence of regulatory connections other than the cyclic repression loop. Finally, the proof does not hold when the equilibrium state is stable because then the spindle shrinks toward the diagonal, so that trajectories can approach the equilibrium. Therefore, it is enough to confirm the instability of the single equilibrium in order to ensure oscillatory behavior in the class of systems that displays only the cyclic repression regulatory connections represented in Fig. 1.

Our simulation results published earlier [18], show that a single extra term $\frac{\alpha_2}{1+w^n}$ in the first equation destroys oscillations. This agrees with our analysis above, which shows that the extra term invalidates the scheme of proof for existence of a cycle. However, we also noticed that for high α, a quite low strength α_2 is sufficient for oscillatory death. As an example, oscillations collapse in the repressilator with $\alpha=500$

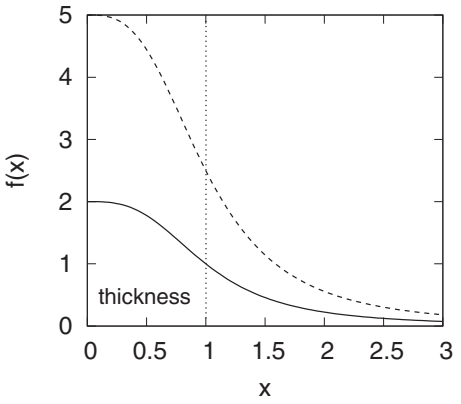

FIG. 7. Thickness of the torus is defined by the decline of the function $f(x)$ and independent of α. The solid and dashed curves show $f(x)$ at $\alpha=2$ and $\alpha=5$, respectively. The vertical line shows the position at which the function declines to a half of the maximal value.

when α_2 is elevated only to 12. We also confirm this sensitivity of the oscillatory mechanism to autoregulatory connections or the uncontrolled expression of genes (α_0). This means that weak regulatory connections can be crucial in defining the dynamics. We can explain this property based on the geometric structure of the phase space.

As α increases, the amplitude of oscillations grows, but the thickness of the torus remains independent of α (Fig. 7). The thickness is defined by the factor $\frac{1}{1+x^n}$, which reflects regulation at the promoters and saturates at low concentrations. As a result, a term that is sufficient to alter the geometric structure depends on α only weakly. This weak dependence is also displayed if an activating connection $\frac{\alpha_1 w^n}{1+w^n}$ is introduced into the u equation: the value for α_1 sufficient for oscillatory death remains low when α increases. For high α, the amplitude of oscillations is much greater than concentrations that saturate the promoters. Therefore, the oscillatory mechanism is sensitive to extra regulatory connections because of the imbalance between the attended concentrations (proportional to α) and those sufficient for saturation of the promoters (defined by $\frac{1}{1+x^n}$).

In a two-dimensional relaxation system, the onset of oscillations as a parameter changes has a clear geometric interpretation: the null clines intersect at an extreme point of one of the null clines. Typically, in systems of nonrelaxation type, this correspondence is lost, but a qualitative one still holds. By contrast, in the repressilator, no qualitative changes in the topology of the phase space seem to correspond to the onset of oscillations. In a repressilator with high parameter α, the torus stretches along the walls of the trapping cube, where one of the variables is near zero (Fig. 5). In particular,

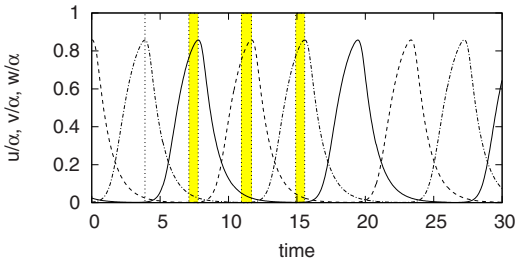

FIG. 8. (Color online) Time series for high α ($\alpha=200$). Note that decreases in each variable occur in both fast and slow phases. The dotted vertical lines correspond to the extrema, at which the trajectory crosses one of the null clines. The shaded intervals correspond to (++−), (−++), and (+−+) octants.

in the octant (+−−) v decreases along with w while u grows. However, the shape of the octant dictates that u remains small, so that u and w decrease at very different rates. Therefore, the difference in the dynamics of all three variables separates the trajectory from the diagonal and makes the equilibrium state unstable.

The dynamics of v and w above are different only due to their distinct rates of decline in the (+−−) octant. At low α, where the equilibrium state *is* stable, the rates of decline are similar, and the trajectory converges to the diagonal. Therefore, an increase in α can be viewed as introducing a time scale separation: the trajectory is close to one of the null clines in each octant, and the corresponding variable remains in quasiequilibrium. However, a fast-decreasing variable will decline slowly in a following octant (Fig. 8); i.e., the time scale separation is temporal or transient. We did not find a coordinate transformation that separates slow and fast variables. Making any one variable permanently slow or fast by introducing a factor in the corresponding equation kills oscillations in the repressilator model [18]. The temporal time scale separation explains the sensitivity of oscillations to scaling of the right-hand side of any one repressilator equation.

Relaxation oscillations are advantageous in synchronization [24]. It may take dozens of oscillatory cycles for smooth oscillators, and just a few cycles for relaxation oscillators to synchronize with a given precision. The property is shown for different types of coupling, including diffusive [25]. We have confirmed it for a pair of diffusively coupled repressilators (Fig. 6). In the case of high α, the repressilators synchronize within a couple of cycles, whereas it takes many cycles in the case of moderate α. The dependence of synchronization on α may display for other types of coupling (e.g., [14,26]). This is a very interesting topic for future studies.

[1] C. H. Ko and J. S. Takahashi, Hum. Mol. Genet. **15**, R271 (2006).
[2] P. Nurse, Cell **100**, 71 (2000).
[3] L. Ma *et al.*, Proc. Natl. Acad. Sci. U.S.A. **102**, 14266 (2005).
[4] K. Tsaneva-Atanasova, C. L. Zimliki, R. Bertram, and A. Sherman, Biophys. J. **90**, 3434 (2006).
[5] M. Kærn, M. Menzinger, R. Satnoianu, and A. Hunding, Faraday Discuss. **120**, 295 (2002).
[6] O. Pourquie, Science **301**, 328 (2003).
[7] M. Atkinson, M. Savageau, J. Myers, and A. Ninfa, Cell **113**, 597 (2003).
[8] T. S. Gardner, C. R. Cantor, and J. J. Collins, Nature (London) **403**, 339 (2000).
[9] M. Elowitz and S. Leibler, Nature (London) **403**, 335 (2000).
[10] A. Becskei and L. Serrano, Nature (London) **405**, 590 (2000).
[11] J. Hasty, D. McMillen, and J. Collins, Nature (London) **420**, 224 (2002).
[12] B. N. Kholodenko, Nature Reviews **7**, 165 (2006).
[13] J. Tyson, K. Chen, and B. Novak, Curr. Opin. Cell Biol. **15**, 221 (2003).
[14] J. Garcia-Ojalvo, M. Elowitz, and S. Strogatz, Proc. Natl. Acad. Sci. U.S.A. **101**, 10955 (2004).
[15] A. Kuznetsov, M. Kaern, and N. Kopell, SIAM J. Appl. Math. **65**, 392 (2004).
[16] N. Barkai and S. Leibler, Nature (London) **403**, 267 (2000).
[17] J. Hasty, F. Isaacs, M. Dolnik, D. McMillen, and J. J. Collins, Chaos **11**, 207 (2001).
[18] D. Yang, Y. Li, and A. Kuznetsov, Chaos **19**, 033115 (2009).
[19] O. Buse, A. Kuznetsov, and R. Pérez, Int. J. Bifurcation Chaos Appl. Sci. Eng. **19**, 4097 (2009).
[20] H. R. Ueda, M. Hagiwara, and H. Kitano, J. Theor. Biol. **210**, 401 (2001).
[21] L. You, R. S. Cox, R. Weiss, and F. N. Arnold, Nature (London) **428**, 868 (2004).
[22] D. McMillen, N. Kopell, J. Hasty, and J. Collins, Proc. Natl. Acad. Sci. U.S.A. **99**, 679 (2002).
[23] V. Afraimovich and S.-B. Hsu, *Lectures on Chaotic Dynamical Systems*, AMS/IP Studies in Advanced Mathematics (AMS, Providence, RI, 2002), p. 20.
[24] D. Somers and N. Kopell, Biol. Cybern. **68**, 393 (1993).
[25] E. Izhikevich, SIAM J. Appl. Math. **60**, 1789 (2000).
[26] E. Ullner, A. Zaikin, E. I. Volkov, and J. Garcia-Ojalvo, Phys. Rev. Lett. **99**, 148103 (2007).